Journal of Systems Engineering and Electronics
Vol. 32, No. 4, August 2021, pp.873 – 880

Range-spread target detector via coherent energy accumulation and block thresholding denoising

ZHANG Yunjian[1], PAN Pingping[1], DENG Zhenmiao[1,*], and WU Gang[2]

1. School of Electronics and Communication Engineering, Sun Yat-sen University, Guangzhou 510275, China;
2. Jiuquan Satellite Launch Center, Dunhuang 736200, China

Abstract: A range-spread target (RST) detector is proposed for wideband radar. The detector, referred to as a conjugate multiplication and block thresholding (CMBT) detector, is simple for implementation in existing radar systems and has the advantage of minor calculation. First, the target energy of adjacent stretched echoes is coherently accumulated via conjugate multiplication and Fourier transform operations. It is noted that conjugate multiplication of two complex Gaussian distributed noise is complex double Gaussian distributed, leading to a signal to noise ratio (SNR) loss. Subsequently, considering the sparsity and clustering characteristics of the conjugate multiplication amplitude spectrum (CMAS), the block thresholding method is adopted for denoising, where the noise and cross-terms are adaptively smoothed, and the signal terms can be basically preserved. Finally, numerical simulation results for both synthetic and real radar data validate the effectiveness of the proposed detector, comparing with the conventional integration detector (ID), the spatial scattering density (SSD) detector, and waveform entropy (WE) and waveform contrast (WC) based detectors.

Keywords: wideband radar, detection, range-spread target, conjugate multiplication, block thresholding denoising.

DOI: 10.23919/JSEE.2021.000075

1. Introduction

Modern high resolution radar could obtain high range resolution and more target information by transmitting wideband waveforms. When the target size is larger than the radar resolution cell, the scatterers distribute over several range cells and the target is regarded as the range-spread target (RST). Since the echo energy is scattered, the signal-to-noise ratio (SNR) in a single range cell is reduced, and therefore, the conventional point target detectors used in low resolution radar systems are no longer applicable.

The issue of RST detection has been the object of great interest over the past several decades [1−3]. A large number of work appeared in the open literature, dealing with the design and performance analysis of suitable detectors in specific settings. The existing RST detectors mainly include the generalized likelihood ratio test (GLRT) [4−12], Rao test [13−17], Wald test [15−18], adaptive subspace detector (ASD) [19], time-frequency decomposition (TFD) [20,21], non-local nonlinear shrinkage map (NLNSM) [22], modified correlation matrix (MCOM) [23], maximal invariant statistic (MIS) [24−26], matched subspace detector (MSD) [27], and singular value decomposition (SVD) [28].

Detectors such as GLRT, Rao test, Wald test, and MIS, all treat the target as a combination of independent point scatterers. The specific detection algorithms based on assumed clutter and noise statistical model incoherently accumulate the target energy. Then the detection statistics are compared with the decision threshold, which is determined by probability of false alarm. The performance of this kind of detectors is satisfactory when the SNR of a single range cell is relatively high. However, when the SNR decreases, the detection performance rapidly decays. ASD and MSD first project noisy signals (and clutter) into different subspaces. Essentially, the corresponding detector belongs to the category of GLRT, and still has the problem of performance degradation under low SNR conditions. Moreover, it is noted that the aforementioned methods regard the radar echo as a combination of isolated scatterers. When there are multiple targets in the echo, these detectors can only determine whether there are targets, but cannot reveal the number and position of targets. TFD and MCOM use the correlation of two or more adjacent pulses for detection, which is equivalent to utilizing the target characteristics of wideband radar, and

Manuscript received August 04, 2020.
*Corresponding author.
This work was supported by the Joint Fund of Aerospace Science and Engineering (76150-41020014), and the Regional Joint Fund for Basic and Applied Basic Research of Guangdong Province (2019B15 15120009).

their performances are improved. The limitation of the TFD detector is that it is only applicable to the assumption that the target range walking is restricted in several range cells. When the target motion parameters are unknown and the target velocity is large, the performance might decline sharply. While the limitation of the MCOM is that it needs a large enough range window for the fast moving target, resulting in an increase in the amount of calculation. The SVD detector studies the RST detection of a single wideband echo embedded in additive white Gaussian noise (AWGN). When the SNR is low, the characteristic value of the noise might be regarded as the harmonic of the target scatterers, which affects the detection performance.

Considering partially homogeneous disturbance environment and target range walking effect, range frequency domain-Rao (RFD-Rao) and -Wald (RFD-Wald) tests are proposed [29], the performance of which outperforms that of some existing detectors. The waveform entropy (WE) based RST detector was proposed in [30]. However, multiple successive high resolution range profiles (HRRPs) are required to calculate the arithmetic average, and the detection performance is affected by high speed targets. In [31], the waveform contrast WC of HRRP was utilized as the test statistic for RST detection. The WC-based detector is then extended to multiple HRRPs [32]. In [33], an RST detector was proposed based on similarity of multiple successive HRRPs, which was measured by Minkowski distance. The detection performance is improved comparing with that of WE and WC detectors. For the aforementioned methods, motion compensation is required. Since the accumulation of signal energy is not achieved, further improvement of detection performance is promising.

In this paper, an RST detector via conjugate multiplication of adjacent stretched pulses and block thresholding denoising, referred to as the CMBT detector, is proposed. It is assumed that the stretched pulse is embedded in AWGN. After conjugate multiplication, however, the noise term is complex double Gaussian distributed, the amplitude probability density function of which is more heavy-tailed than that of the Rayleigh distribution. This is unfavorable for detection, since when the probability of false alarm is constant, it is necessary to increase the decision threshold, which leads to the decrease of probability of detection. Considering the sparsity and clustering characteristic of the conjugate multiplication amplitude spectrum (CMAS), a block thresholding strategy is adopted for denoising [34]. The block-by-block thresholding procedure utilizes information about neighboring wavelet coefficients and allows the balance between variance and bias to be varied along the curve. The block size and thresholding constant are adaptively chosen to achieve both globally and locally optimal estimation accuracy. After denoising, the noise term is adaptively smoothed and the signal term is basically preserved. The numerical results from synthetic and real radar data show that the proposed detector achieves a better performance, compared with the conventional integration detector (ID) and the spatial scattering density (SSD) detector [12].

2. Signal model

It is supposed that the radar transmits a train of chirp pulses. The complex envelope of the transmitted pulse is expressed as

$$s(t)=\mathrm{rect}\left(\frac{t}{T}\right)\exp(\mathrm{j}\pi\gamma t^2) \tag{1}$$

where $\mathrm{rect}(u)=\begin{cases}1, & |u|<1/2\\ 0, & \text{otherwise}\end{cases}$ is the rectangle pulse shape, T is the pulse width, and γ is the chirp rate. After modulating the carrier signal by $s(t)$, the transmitted signal is

$$s_t(\hat{t},t)=s(\hat{t})\exp(\mathrm{j}2\pi f_c\hat{t}) \tag{2}$$

where f_c is the carrier frequency, $\hat{t}=t-t_m$ is the fast time, $m=-M,\cdots,M$ is the index number of the transmitted pulse in a coherent processing interval (CPI), t is the full time, $t_m=mT_r$ is the slow time, where T_r is the pulse repetition interval (PRI). Under the stop-and-go assumption, i.e., the motion parameters of the targets are regarded as constant within the pulse duration, the received signal of the wideband LFM radar is represented as

$$s_{\mathrm{re}}(t,t_m)=\sum_{p=0}^{P-1}A_p s[t-\tau_p(t_m)]\cdot \exp[\mathrm{j}2\pi f_c[t-\tau_p(t_m)]]+\omega(t,t_m) \tag{3}$$

where P is the number of scatterers, A_p is the backward scattering coefficient of the pth scatterer, $\omega(t,t_m)$ is the complex AWGN, and the round-trip time delay $\tau_p(t_m)$ is expressed as

$$\tau_p(t_m)=\frac{2R_p(t_m)}{\mathrm{c}} \tag{4}$$

where $R_p(t_m)$ is the distance between the radar and the pth scatterer at slow time t_m, and c is the speed of light. In wideband radar systems, due to the large bandwidth of signal, the stretching is often adopted for pulse compression instead of matched filtering. The local reference signal for stretching is written as

$$s_{\mathrm{lo}}(t)=\mathrm{rect}\left(\frac{t}{\hat{T}}\right)\exp[-\mathrm{j}(2\pi f_c t+\pi\gamma t^2)] \tag{5}$$

where $\hat{T}$ denotes the length of the received window, which should be longer than the pulse duration. The stretched signal is obtained by

$$s_{\mathrm{st}}(t,t_m)=s_{\mathrm{re}}(t,t_m)\cdot s_{\mathrm{lo}}(t)=\sum_{p=1}^{P}A_p\mathrm{rect}\left[\frac{t-\tau_p(t_m)}{T}\right]\cdot$$
$$\exp\left[-\mathrm{j}2\pi\tau_p(t_m)\gamma t\right]\cdot\exp\left[-\mathrm{j}2\pi f_c\tau_p(t_m)\right]+\omega_1(t,t_m)=$$
$$s_{\mathrm{sig}}(t,t_m)+\hat{\omega}(t,t_m) \tag{6}$$

where $s_{\mathrm{sig}}(t,t_m)$ is the signal term, and $\hat{\omega}(t,t_m)=\omega(t,t_m)\cdot s_{\mathrm{lo}}(t)$ is the noise term after stretching, which is still Gaussian distributed. It is noted that the exponential terms including $\tau_p^2(t_m)$ are ignored in (6) since they are approximately equal to 1 in general.

3. Proposed detection algorithm

3.1 Coherent accumulation method

In practical wideband radar systems, consecutive echoes are highly correlated in amplitude since they share almost the same scattering center model, and therefore, the energy of which can be accumulated. To coherently accumulate the energy, the stretched signal at t_m is multiplied with the conjugate of the adjacent stretch signal at t_{m+1}, then we obtain

$$s_{\mathrm{cm}}(t,t_m)=s_{\mathrm{st}}(t,t_m)\cdot s_{\mathrm{st}}^*(t,t_{m+1})=$$
$$s_{\mathrm{s}}(t,t_m)+s_{\mathrm{c}}(t,t_m)+\tilde{\omega}(t,t_m) \tag{7}$$

where $(\cdot)^*$ denotes the conjugation operator, the self-term $s_{\mathrm{s}}(t,t_m)$ indicates the conjugate product of adjacent echoes from the same scatterer, the cross-term $s_{\mathrm{c}}(t,t_m)$ indicates the conjugate product of adjacent echoes from the different scatterers, and $\tilde{\omega}(t,t_m)$ is the noise term after conjugate multiplication, which is complex double Gaussian distributed [35]. It was derived in [35] that the marginal distribution of product of two independent zero-mean complex Gaussian random variables is expressed as

$$f_{R_z,\Theta_z}(r_z,\theta_z)=\frac{4r_z}{\sigma_x^2\sigma_y^2}K_0\left(\frac{2r_z}{\sigma_x\sigma_y}\right) \tag{8}$$

where $R_z=|XY|$, $X\sim\mathcal{CN}(0,\sigma_x^2)$, $Y\sim\mathcal{CN}(0,\sigma_y^2)$, $\Theta_z=\arg Z\in[0,2\pi)$ is the phase of Z, and $K_0(z)$ is the modified Bessel function of the second kind with order 0 and argument z.

According to (7), after conjugate multiplication of adjacent stretched signals, the noise variance becomes $\sigma_{\mathrm{cm}}^2=2A^2\sigma^2+\sigma^4$, where σ^2 is the noise variance of the stretched signal before conjugate multiplication, and A is the backscattering intensity of the target. Then, the SNR after conjugate multiplication is computed as

$$\mathrm{SNR}_{\mathrm{cm}}=\frac{A^4}{2A^2\sigma^2+\sigma^4}=\frac{\mathrm{SNR}_{\mathrm{ori}}^2}{1+2\mathrm{SNR}_{\mathrm{ori}}} \tag{9}$$

where $\mathrm{SNR}_{\mathrm{ori}}$ is the SNR before conjugate multiplication. The relationship between $\mathrm{SNR}_{\mathrm{ori}}$ and $\mathrm{SNR}_{\mathrm{cm}}$ is shown in Fig. 1. It is seen that $\mathrm{SNR}_{\mathrm{cm}}$ is approximately −4.7 dB when $\mathrm{SNR}_{\mathrm{ori}}$ is 0 dB. When $\mathrm{SNR}_{\mathrm{ori}}<0$ dB, the loss rate increases gradually with the decrease of $\mathrm{SNR}_{\mathrm{ori}}$. This is the reason that the block denoising procedure is introduced. Considering the clustering characteristic of HRRP, the noise in the target-absence range cells can be significantly suppressed (as shown in Section 4), and therefore, the SNR threshold for detection is reduced.

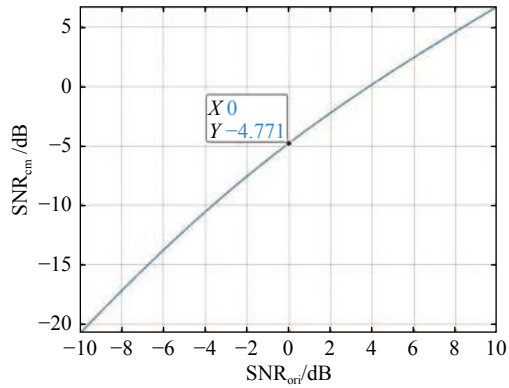

Fig. 1 Relationship between the SNR after conjugate multiplication ($\mathrm{SNR}_{\mathrm{cm}}$) and the SNR of stretched signal ($\mathrm{SNR}_{\mathrm{ori}}$)

Specifically, the three terms on the right-hand side of (7) are expressed as

$$s_{\mathrm{s}}(t,t_m)=\sum_{p=1}^{P}A_p^2\mathrm{rect}\left[\frac{t-\tau_p(t_m)}{T}\right]\mathrm{rect}\left[\frac{t-\tau_p(t_{m+1})}{T}\right]\cdot$$
$$\exp\left[\mathrm{j}2\pi\gamma[\tau_p(t_{m+1})-\tau_p(t_m)]t\right]\cdot$$
$$\exp\left[\mathrm{j}2\pi f_c[\tau_p(t_{m+1})-\tau_p(t_m)]\right], \tag{10}$$

$$s_{\mathrm{c}}(t,t_m)=\sum_{q=1}^{P}\sum_{p=1,p\neq q}^{P}A_pA_q\mathrm{rect}\left[\frac{t-\tau_q(t_m)}{T}\right]\cdot$$
$$\mathrm{rect}\left[\frac{t-\tau_p(t_{m+1})}{T}\right]\exp\left[\mathrm{j}2\pi\gamma[\tau_p(t_{m+1})-\tau_q(t_m)]t\right]\cdot$$
$$\exp\left[\mathrm{j}2\pi f_c[\tau_p(t_{m+1})-\tau_q(t_m)]\right], \tag{11}$$

$$\tilde{\omega}(t,t_m)=\hat{\omega}(t,t_m)s_{\mathrm{sig}}^*(t,t_{m+1})+$$
$$\hat{\omega}^*(t,t_{m+1})s_{\mathrm{sig}}(t,t_m)+\hat{\omega}(t,t_m)\hat{\omega}^*(t,t_{m+1}). \tag{12}$$

Then, employing the Fourier transform (FT) to $s_{\mathrm{cm}}(t,t_m)$, we obtain the conjugate multiplication spectrum (CMS) of adjacent stretched echoes,

$$S_{\mathrm{cm}}(f,t_m)=S_{\mathrm{s}}(f,t_m)+S_{\mathrm{c}}(f,t_m)+\tilde{W}(f,t_m)=$$
$$S(f,t_m)+\tilde{W}(f,t_m) \tag{13}$$

where $S(f,t_m)$ is the noise-free signal consisting of self-terms and cross-terms of the target, and $\tilde{W}(f,t_m)$ represents the frequency domain noise. The SNR for pulse t_m is defined as

$$\mathrm{SNR}_m=10\lg\left(\frac{\|S(f,t_m)\|_2^2}{L\sigma^2}\right) \tag{14}$$

where L is the number of range cells occupied by the target, and σ^2 is the power of noise $\tilde{W}(f,t_m)$. Taking the absolute value of (12), we obtain the CMAS, which is expressed as

$$r(f,t_m) \triangleq |S_{\mathrm{cm}}(f,t_m)| = |S(f,t_m)| + |\tilde{W}(f,t_m)|. \tag{15}$$

3.2 Denoising

According to the sparsity and clustering characteristic of the CMAS, a block thresholding method is adopted for denoising [34]. Block thresholding can be regarded as an automatic hypothesis test, which selects a set of important variables (wavelet coefficients) by omitting insignificant ones and fits to the data a model consisting of only the important variables. In other words, a block thresholding estimator thresholds wavelet coefficients in groups instead of individually. Comparing with hard and soft thresholding methods, the estimation accuracy of block thresholding can be improved by utilizing information about neighboring wavelet coefficients and making simultaneous decisions on all the coefficients within a block.

The procedure of block thresholding is summarized as follows:

(i) Transform the noisy data via the wavelet transform.

(ii) At each resolution level, the wavelet coefficients are divided into nonoverlapping blocks. If the sum of the squared coefficients in a block is larger than the optimal threshold, then the coefficients are retained, otherwise the coefficients are discarded.

(iii) Taking the inverse wavelet transform to the coefficients produced by (ii), the estimated (denoised) signal is obtained.

Supposing a noisy CMAS from adjacent pulses is available, define $R=\{r(f_i)\}$, $i=1,2,\cdots,N(=2^J)$, where the slow time index t_m is ignored. Let $\tilde{R}=W\cdot R/\sqrt{N}$ be the discrete wavelet transform of $R/\sqrt{N}$, which is written as

$$\tilde{R}=(\tilde{\xi}_{j_0 1},\cdots,\tilde{\xi}_{j_0 2^{j_0}},\tilde{r}_{j_0 1},\cdots,\tilde{r}_{j_0 2^{j_0}},\tilde{r}_{J-1,1},\cdots,\tilde{r}_{J-1,2^{J-1}}) \tag{16}$$

where $\tilde{\xi}_{j_0 k}$ is the gross structure term at the lowest resolution level, and $\tilde{r}_{j,k}$ $(j=1,\cdots,J-1,\ k=1,\cdots,2^j)$ is the empirical wavelet coefficient at level j which represent the detail structure at scale $2j$. The output of the denoising process is given by

$$r_{\mathrm{o}}(f)=\sum_{k=1}^{2^{j_0}}\tilde{\xi}_{j_0 k}\phi_{j_0 k}(f)+\sum_{j=j_0}^{J-1}\sum_{b}\left(\sum_{k\in(jb)}\tilde{r}_{j,k}\psi_{j,k}(f)\right)I(S_{jb}^2>\lambda L\sigma^2/\sqrt{N}) \tag{17}$$

where $\phi_{j,k}(f)=2^{j/2}\phi(2^j f-k)$, $\psi_{j,k}(f)=2^{j/2}\psi(2^j f-k)$, and $\{\phi,\psi\}$ is a pair of father and mother wavelets. L and λ are the block size and the thresholding constant, respectively. $S_{jb}^2=\sum_{k\in(jb)}\tilde{r}_{j,k}^2$ denotes the sum of squares of the empirical coefficients in the block. σ^2 is the noise variance, and $I(\cdot)$ is the unit step function. See [29] for more details.

3.3 Detection algorithm

The detection problem here is to decide whether the radar echoes are target-present ($\mathcal{H}_1$ hypothesis) or target-free ($\mathcal{H}_0$ hypothesis) using two adjacent stretched pulses. The binary hypothesis test is expressed as

$$\begin{cases}\mathcal{H}_1:\ r_{\mathrm{o}}(f)=s(f)+\omega(f)\\ \mathcal{H}_0:\ r_{\mathrm{o}}(f)=\omega(f)\end{cases} \tag{18}$$

where f is the frequency index of the denoised CMAS. The proposed decision strategy is simply written as

$$\Lambda(r)=\max_f|r_{\mathrm{o}}(f)|\underset{\mathcal{H}_0}{\overset{\mathcal{H}_1}{\gtrless}}T \tag{19}$$

where T is the detection threshold to be set according to the desired value of the probability of false alarm P_{FA}. To determine the relationship between T and P_{FA}, it is necessary to analyze the characteristic of the noise term. However, owing to the FT of complex double Gaussian distribution, modulus, and block thresholding denoising, it is difficult to derive the closed-form expression. Therefore, the Monto Carlo tests are adopted to calculate the detection threshold. The block diagram of the proposed detector is shown in Fig. 2.

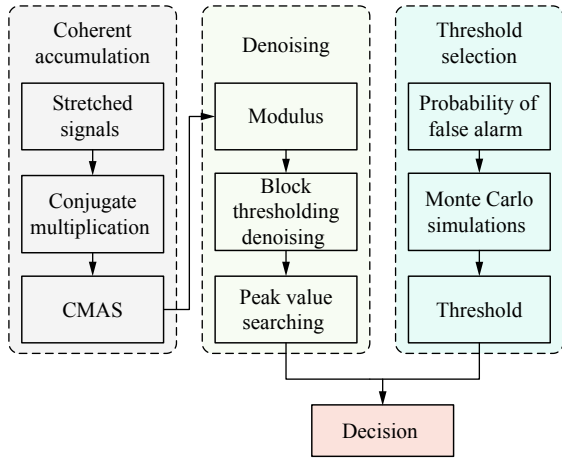

Fig. 2 Block diagram of the proposed detector

3.4 Calculation analysis

The total amount of calculation of the detection algorithm can be divided into three parts: (i) conjugate multiplication of adjacent stretched signals; (ii) FT of conjugate multiplication signals; (iii) block thresholding de-

noising procedure. Suppose the length of stretched signals is N, the computational complexity of the first part is $O(N)$. Then, the fast FT (FFT) is applied to the conjugate multiplication signal, the computational complexity of which is $O(N\log_2 N)$. For the block thresholding denoising, it is demonstrated that it can be implemented at a computational cost of $O(N)$ [34]. Therefore, the total computational complexity of the proposed detector is $O(N+N\log_2 N)\log N)$. For some correlation-based methods, e.g., [23] and [33], FFT of each stretched pulse and cross-correlation of two or more pulses are necessary, leading to the computational complexity of $O(N^2+N\log_2 N)$ at least.

4. Numerical simulations

4.1 Illumination of energy accumulation and denoising

First, an experiment using synthetic data are performed to evaluate the energy accumulation effect. The transmitted waveform is chirp, and AWGN is added to the stretched echo. Table 1 lists the detailed simulation parameters. The target #1 is set as an aircraft model containing 17 scatterers, with a target length of 13 m. Target velocity is 1 000 m/s, and the acceleration is ignored. Target #2 is set as a four-axis unmanned aerial vehicle (UAV) model contains 56 scatterers, with a velocity of 50 m/s and an acceleration of 2.5 m/s^2.

Table 1 Simulation parameters

Parameter	Value
Center frequency/GHz	9
Bandwidth/GHz	1
Pulse width/μs	100
Sampling frequency/GHz	1
PRF/Hz	50
Target #1 (aircraft) initial distance/m	16 000
Target #1 (aircraft) velocity/(m/s)	1 000
Target #1 (aircraft) acceleration/(m/s^2)	0
Target #2 (UAV) initial distance/m	1 000
Target #2 (UAV) velocity/(m/s)	50
Target #2 (UAV) acceleration/(m/s^2)	2.5

The energy concentration of the conjugate multiplication operation is investigated at a relatively high SNR level, e.g., 10 dB. The CAMS of two adjacent pulses is shown in Fig. 3, using the black solid line. The results for aircraft and UAV are respectively shown in Fig. 3(a) and Fig. 3(b). It is clear that the energy of different scatterers is focused on the main peak. Then, the block thresholding denoising is applied to the CMAS. Comparative results are also shown in Fig. 3, using the red solid line. For the aircraft model, it is seen that the self-term and cross-terms are essentially preserved and the noise terms are substantially suppressed. While for the UAV model, there exists a large number of cross-terms in the CMAS before the denoising procedure. After the block thresholding denoising, however, it is seen that relatively weak cross-terms are significantly suppressed. Also, the noise is smoothed, and the target energy is basically preserved.

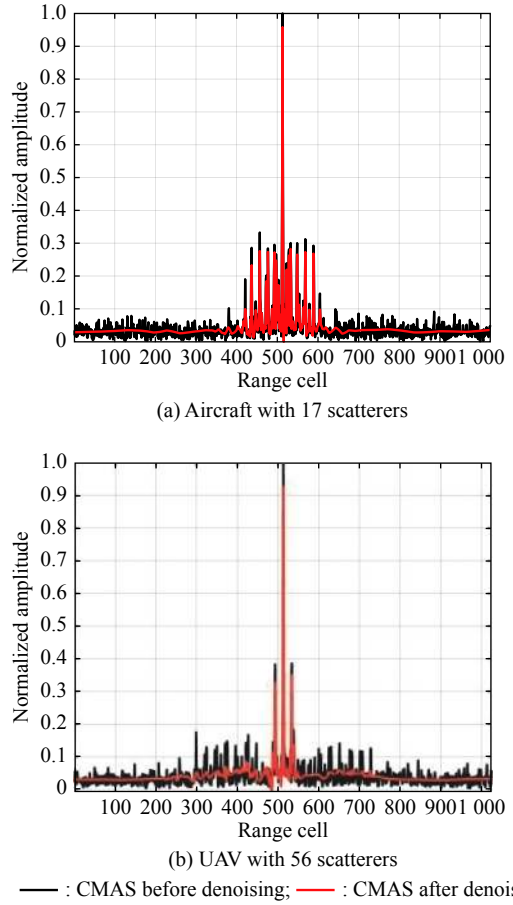

Fig. 3 Illumination of energy concentration using conjugate multiplication, and denoising effect using block thresholding

4.2 Performance evaluation of the proposed CMBT detector

Next, the performance of the proposed CMBT detector is evaluated by using both synthetic and real data, compared with that of the conventional ID and of the SSD detector. The ID uses the energy of the noisy HRRP $S_{\mathrm{st}}(f)$, i.e., the FT of (6), in the whole range window, which is given by

$$\frac{1}{\sigma^2}\sum_f |S_{\mathrm{st}}(f)|^2 \underset{\mathcal{H}_0}{\overset{\mathcal{H}_1}{\gtrless}} T_d \tag{20}$$

where σ^2 is the noise variance, and T_d is the detection threshold. The SSD-GLRT detector is expressed [12] as

$$\sum_f \ln\left[1+\frac{\zeta}{1-\zeta}\mathrm{e}^{|S_{\mathrm{st}}(f)|^2/\sigma^2}\right]\underset{\mathcal{H}_0}{\overset{\mathcal{H}_1}{\gtrless}} T_s \tag{21}$$

where T_s is the detection threshold, and ζ is a parameter chosen to control the spatial density of the scatterers. Here, the optimal parameter of ζ is chosen as 17/1 024 for synthetic data (the aircraft model). The receiver operation curves (ROCs) for the three detectors are shown in Fig. 4. It is seen that the proposed detector achieves the best performance among all three detectors.

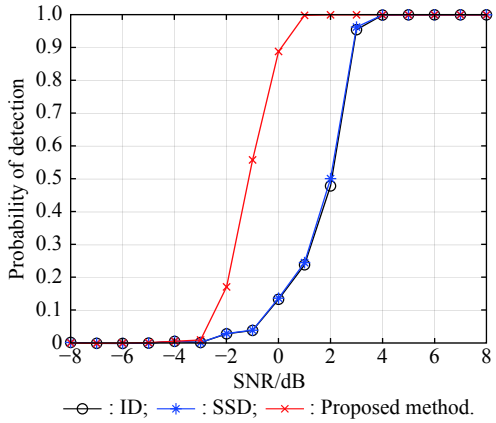

Fig. 4 Performance comparison of ID, SSD, and the proposed CMBT detector for false alarm probability 10^{-3}, using synthetic data

Also, we use the real radar data to validate the performance of our proposed detector. The radar carrier frequency is 11.5 GHz, the PRF is 100 Hz, and the bandwidth is 3 GHz, correspondingly the range resolution is 0.05 m. The target is a civil aircraft and the length is approximately 37 m. Each HRRP contains 2 048 range cells. The HRRPs of the first two pulses, of the second and the third pulses, and the corresponding CMASs are shown in Fig. 5 and Fig. 6, respectively. The SNR for this group of data is high, that is, the estimated SNR is 25.2 dB. Therefore, we add complex AWGN with different variances to the HRRP for performance evaluation. We additionally compare the performance of the proposed detector with that of WE [30] and WC [31] detectors.

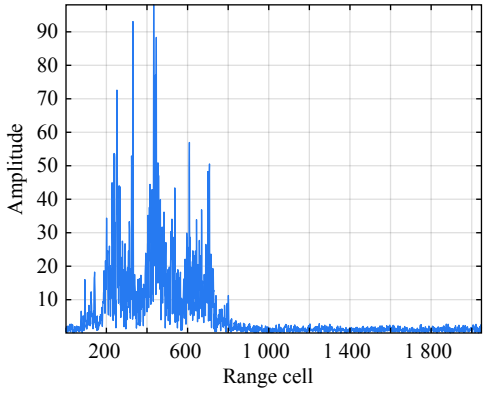

(a) HRRP of the first pulse

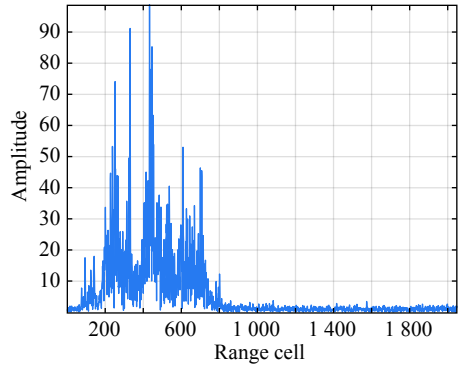

(b) HRRP of the second pulse

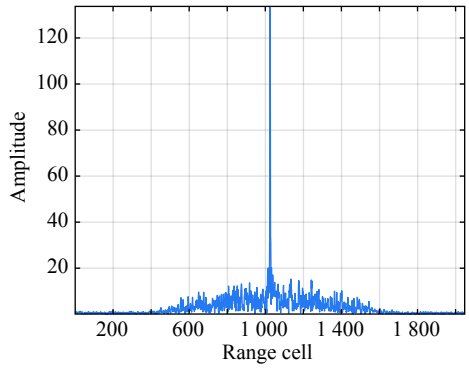

(c) CMAS of the first and second pulses

Fig. 5 Illumination of energy accumulation effect for the first two pulses of real radar data

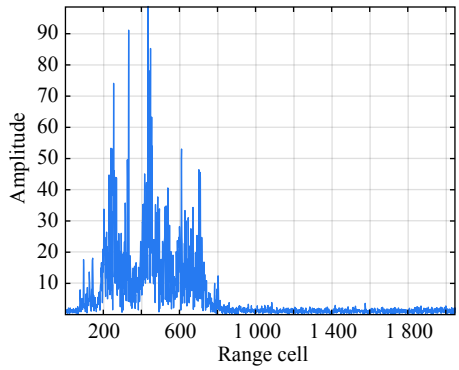

(a) HRRP of the second pulse

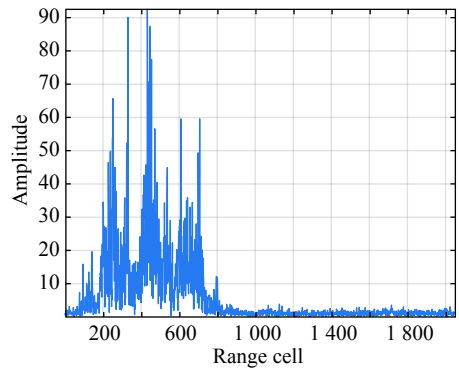

(b) HRRP of the third pulse

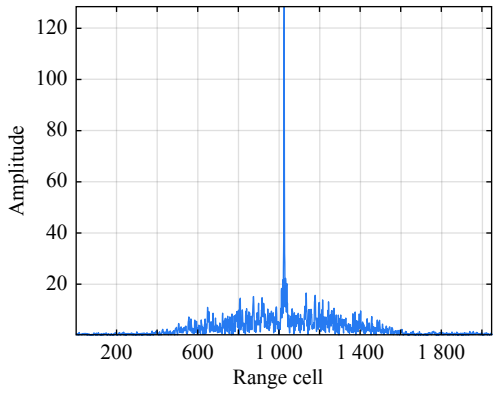

(c) CMAS of the second and the third pulses

Fig. 6 Illumination of energy accumulation effect for the second and the third pulses of real radar data

The detection results using 4 000 pulses are shown in Fig. 7. It is seen that the SNR threshold of the proposed CMBT detector outperforms that of the other four detectors, which demonstrates the effectiveness and improvement of the proposed method.

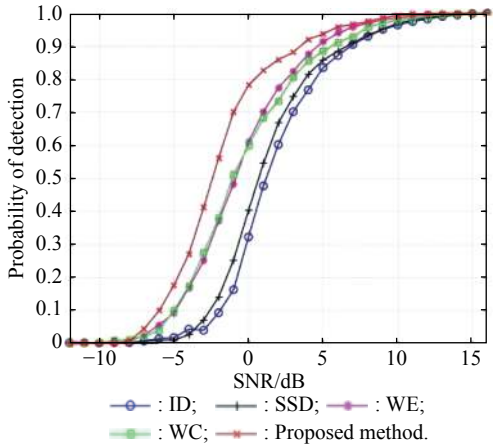

Fig. 7 Performance comparison of ID, SSD, WE, WC, and the proposed CMBT detector for false alarm probability 10^{-3}, using real radar data

5. Conclusions

In this paper, we develop a wideband detector to detect RST in white complex Gaussian noise background. Due to the strong correlation of adjacent echoes, the energy is coherently accumulated by conjugate multiplication. Then the CMAS is obtained by applying FFT. Considering the clustering and sparsity of the CMAS, the block thresholding denoising is adopted. The proposed CMBT detector is simple for implementation in existing radar systems and has the advantage of minor calculation. The experimental results to both synthetic and real radar data verify the improvement of the proposed detector. The performance of the CMBT detector can be further improved, by considering the energy accumulation for multiple adjacent pulses. This idea would be investigated in further works.

References

[1] CHANG J Y, FU X J, JIANG W, et al. Wideband radar detector based on characteristic parameters of echoes. Journal of Systems Engineering and Electronics, 2019, 30(5): 897–904.

[2] CHANG J Y, FU X J, JIANG W, et al. Design of high-performance energy integrator detector for wideband radar. Journal of Systems Engineering and Electronics, 2019, 30(6): 1110–1118.

[3] XU S W, SHUI P L. Performance analysis of multi-channel order statistics detector for range-spread target. Journal of Systems Engineering and Electronics, 2012, 23(5): 689–699.

[4] BANDIERA F, BESSON O, RICCI G. Adaptive detection of distributed targets in compound-Gaussian noise without secondary data: a Bayesian approach. IEEE Trans. on Signal Processing, 2011, 59(12): 5698–5708.

[5] LEE S, NGUYEN M, SONG I, et al. Detection schemes for range-spread targets based on the semidefinite problem. IEEE Trans. on Aerospace and Electronic Systems, 2018, 55(1): 57–69.

[6] GAO Y C, LI H B, HIMED B. Knowledge-aided range-spread target detection for distributed MIMO radar in non-homogeneous environments. IEEE Trans. on Signal Processing, 2016, 65(3): 617–627.

[7] GAO Y C, LIAO G S, LIU W J. High-resolution radar detection in interference and nonhomogeneous noise. IEEE Signal Processing Letters, 2016, 23(10): 1359–1363.

[8] AUBRY A, DE M A, PALLOTTA L, et al. Radar detection of distributed targets in homogeneous interference whose inverse covariance structure is defined via unitary invariant functions. IEEE Trans. on Signal Processing, 2013, 61(20): 4949–4961.

[9] DAI F Z, LIU H W, SHUI P L, et al. Adaptive detection of wideband radar range spread targets with range walking in clutter. IEEE Trans. on Aerospace and Electronic Systems, 2012, 48(3): 2052–2064.

[10] HE Y, JIAN T, SU F G, et al. Novel range-spread target detectors in non-Gaussian clutter. IEEE Trans. on Aerospace and Electronic Systems, 2010, 46(3): 1312–1328.

[11] CONTE E, DE M A, RICCI G. GLRT-based adaptive detection algorithms for range-spread targets. IEEE Trans. on Signal Processing, 2001, 49(7): 1336–1348.

[12] GERLACH K, STEINER M J. Adaptive detection of range distributed targets. IEEE Trans. on Signal Processing, 1999, 47(7): 1844–1851.

[13] LIU W J, LIU J, HUANG L, et al. Rao tests for distributed target detection in interference and noise. Signal Processing, 2015, 117: 333–342.

[14] SHI B, HAO C P, HOU C H, et al. Parametric Rao test for multichannel adaptive detection of range-spread target in partially homogeneous environments. Signal Processing, 2015, 108: 421–429.

[15] HAO C P, MA X C, SHANG X Q, et al. Adaptive detection of distributed targets in partially homogeneous environment with Rao and Wald tests. Signal Processing, 2012, 92(4): 926–930.

[16] GUAN J, ZHANG X L. Subspace detection for range and Doppler distributed targets with Rao and Wald tests. Signal Processing, 2011, 91(1): 51–60.

[17] CONTE E, DE M A. Distributed target detection in compound-Gaussian noise with Rao and Wald tests. IEEE Trans.

on Aerospace and Electronic Systems, 2003, 39(2): 568–582.
[18] LIU W J, LIU J, LI H, et al. Multichannel signal detection based on Wald test in subspace interference and Gaussian noise. IEEE Trans. on Aerospace and Electronic Systems, 2018, 55(3): 1370–1381.
[19] LEI S W, ZHAO Z Q, NIE Z P, et al. A CFAR adaptive subspace detector based on a single observation in system-dependent clutter background. IEEE Trans. on Signal Processing, 2014, 62(20): 5260–5269.
[20] SHUI P L, LIU H W, BAO Z. Range-spread target detection based on cross time-frequency distribution features of two adjacent received signals. IEEE Trans. on Signal Processing, 2009, 57(10): 3733–3745.
[21] ZUO L, LI M, ZHANG X W, et al. CFAR detection of range-spread targets based on the time-frequency decomposition feature of two adjacent returned signals. IEEE Trans. on Signal Processing, 2013, 61(24): 6307–6319.
[22] XU S W, SHUI P L. Range-spread target detection using 2D non-local nonlinear shrinkage map. Signal Processing, 2014, 98: 337–343.
[23] SHUI P L, XU S W, LIU H W. Range-spread target detection using consecutive HRRPs. IEEE Trans. on Aerospace and Electronic Systems, 2011, 47(1): 647–665.
[24] CIUONZO D, DE M A, ORLANDO D. On the statistical invariance for adaptive radar detection in partially homogeneous disturbance plus structured interference. IEEE Trans. on Signal Processing, 2016, 65(5): 1222–1234.
[25] DE M A, ORLANDO D. Adaptive radar detection of a subspace signal embedded in subspace structured plus Gaussian interference via invariance. IEEE Trans. on Signal Processing, 2015, 64(8): 2156–2167.
[26] CIUONZO D, ORLANDO D, PALLOTTA L. On the maximal invariant statistic for adaptive radar detection in partially homogeneous disturbance with persymmetric covariance. IEEE Signal Processing Letters, 2016, 23(12): 1830–1834.
[27] LIU J, ZHANG Z J, CAO Y H, et al. Distributed target detection in subspace interference plus Gaussian noise. Signal Processing, 2014, 95: 88–100.
[28] TIVIVE F H C, BOUZERDOUM A, AMIN A G. A subspace projection approach for wall clutter mitigation in through-the-wall radar imaging. IEEE Trans. on Geoscience and Remote Sensing, 2014, 53(4): 2108–2122.
[29] WANG Y, CAO Y H, SU H T, et al. RFD-Rao and RFD-Wald tests for distributed targets with range walking effect. Journal of Central South University, 2018, 25(6): 1437–1446.
[30] XU S W, SHUI P L, YAN X. CFAR detection of range-spread target in white Gaussian noise using waveform entropy. Electronics Letters, 2010, 46(9): 647–649.
[31] YANG X L, WEN G J, MA C H, et al. CFAR detection of moving range-spread target in white Gaussian noise using waveform contrast. IEEE Geoscience and Remote Sensing Letters, 2016, 13(2): 282–286.
[32] XU S W, SHI X Y, XUE J, et al. Maneuvering range-spread target detection in white Gaussian noise using multiple-pulse combined waveform contrast. Proc. of the IEEE International Conference on Signal Processing, Communications and Computing, 2017: 1−5.
[33] XU S W, ZHU J N, SHI X Y, et al. CFAR detection of range-spread target in white Gaussian noise based on the discrepancy of distance of successive HRRPs. Proc. of the IEEE International Conference on Signal Processing, Communications and Computing, 2018: 1–5.
[34] CAI T T. On block thresholding in wavelet regression: adaptivity, block size, and threshold level. Statistica Sinica, 2002, 12(4): 1241–1273.
[35] O'DONOUGHUE N, MOURA J M F. On the product of independent complex Gaussians. IEEE Trans. on Signal Processing, 2011, 60(3): 1050–1063.

Biographies

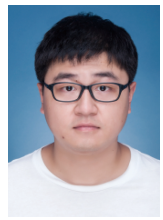

ZHANG Yunjian was born in 1986. He received his B.E. degree in communication engineering from Beijing University of Posts and Telecommunications, Beijing, China, in 2008, M.S. degree in electronics and communication engineering from University of Electronic Science and Technology of China, Chengdu, China, in 2013, and Ph.D. degree in communication and information systems from Xiamen University (XMU), Xiamen, China, in 2016. From 2017 to 2019 he was a post-doctoral research fellow with the School of Information Science and Engineering, XMU. In 2019 he joined the School of Electronics and Communication Engineering, Sun Yat-sen University, China, where he is now an assistant professor. His research interests include statistical signal processing, parameter estimation, and target detection.
E-mail: zhangyunj@mail.sysu.edu.cn

PAN Pingping was born in 1990. She received her B.E. degree in telecommunication engineering and management from Beijing University of Posts and Telecommunications, Beijing, China, in 2012, M.S. degree in communication and information systems from Xiamen University, Xiamen, China, in 2016. She is currently pursuing her Ph.D. degree with the School of Electronics and Communication Engineering, Sun Yat-sen University, China. Her research interests include parameter estimation and signal processing.
E-mail: pingping_pan2008@163.com

DENG Zhenmiao was born in 1977. He received his B.S. degree in electronic engineering and Ph.D. degree in signal and information processing from Nanjing University of Aeronautics and Astronautics (NUAA), Nanjing, China, in 1999 and 2007, respectively. From 2007 to 2009, he was a post doctoral research fellow with the College of Automation Engineering, NUAA, involved in the field of signal detection and parameter estimation. From 2010 to 2019, he was on the faculty of Xiamen University, China, where he has been a full professor since 2016. In 2019, he joined the School of Electronics and Communication Engineering, Sun Yat-sen University, China. His current research interests include signal detection, parameter estimation, array signal processing, and multirate signal processing.
E-mail: dengzhm7@sysu.edu.cn

WU Gang was born in 1980. He received his B.E. degree in measurement and control technology and instrument from Nanjing University of Aeronautics and Astronautics, Nanjing, China, in 2003, and M.S. degree in electronic and communication engineering from Xidian University, Xi'an, China, in 2012. His current research interests include target detection and recognition.
E-mail: 37192275@qq.com